Validation of a numerical model of oxy-fuel combustion in laminar and turbulent jet flames by direct prediction of experimental quantities

Meor F. Zulkifli[*, 1], Franziska Hunger[2], Christian Hasse[2], Frank Beyrau[3], Benjamin A.O. Williams[1]

[1]Department of Mechanical Engineering, Imperial College London, United Kingdom
[2]Chair of Numerical Thermo-Fluid Dynamics, ZIK Virtuhcon, Technische Universitat Bergakademie Freiberg, Germany
[3]Department of Technical Thermodynamics, Otto-von-Guericke-Universitat Magdeburg, Germany

Abstract

An experimental study of non-premixed oxy-fuel jet flames in a co-flow burner is used to validate a numerical model by prediction of directly measureable quantities. Both laminar and turbulent flames were tested, using fuel (17.5% CH_4, 40% CO_2, 42.5% H_2) and oxidiser (68% O_2, 32% CO_2). A simultaneous Rayleigh scattering and OH-PLIF laser diagnostics system was used to recover data from the flames. The corresponding numerical system was computed using an in-house OpenFOAM LES model, and the resulting temperature and compositional data used to predict Rayleigh signals. Tests in laminar conditions enabled the correct selection of kinetic mechanism and radiation and diffusion models. Turbulent simulations incorporated the flamelet progress variable (FPV) approach in the LES framework, and recovered the Rayleigh signal by treating it as an additional scalar value. The resulting comparison between numerical and experimental data shows good agreement, and the overall confidence in the validation of the model is significantly improved because the "traditional" measurement assumptions are avoided, enabling future investigations of a broad range of oxy-fuel systems.

Introduction

Fossil fuels will remain an important energy source for the foreseeable future and combustion processes will continue to result in the production of carbon dioxide (CO_2) emissions. The accumulation of evidence that climate change is to a large part due to this emission has led to the establishment of several parties such as Intergovernmental Panel on Climate Change (IPCC) to prepare scientific assessments of the CO_2 risk, and also the Kyoto Protocol being a treaty that sets a limitation or reduction of CO_2 emission to industrialised countries.

Wall et al [1] has proposed several technologies to reduce CO_2 emission which are known as pre-combustion capture, post-combustion capture, and also oxy-fuel combustion. However, oxy-fuel combustion stands out as the most promising and efficient carbon capture and storage (CCS) method, with the most potential [2]. In oxy-fuel combustion, the air that is usually used in combustion, containing nitrogen, is replaced by pure oxygen and if a lower temperature flame is required, flue gas is added. The final product of this combustion will be CO_2 and water vapour, where CO_2 can be easily separated through a condensation process allowing the CO_2 to be easily captured and stored or recycled [3].

This type of flame is not well characterised, and the complexity of the flame due to the substitution of N_2 to CO_2 results in high soot formation [4], heat losses [5], and significantly altered chemical paths [6, 7, 8]. When combined with a fuel mixture that contains high diffusivity molecule such as H_2 extra challenges are introduced when collecting, interpreting and comparing the experimental data to the numerical simulations. This becomes more complex when a high temperature flame is investigated as the CO_2 tends to dissociate generating excess CO which is a particular problem when acquiring two-dimensional temperature data using Rayleigh scattering. Post-processing the data to find a desired physical quantity such as temperature for comparison with numerical simulation becomes impossible as the evaluation of Rayleigh scattering by directly converting the Rayleigh signal to temperature is prone to inaccuracy due to the variation of effective Rayleigh cross section with position.

However, an approach suggested by Connelly et al. [9] to directly compare the signal measured in the experiment to the numerical simulation becomes feasible as experimental errors could be reduced and hence the signal to noise ratio could definitely be increased. In this experiment, this approach will be applied to validate a numerical model of oxy-fuel combustion in laminar and turbulent jet flames by using laser Rayleigh scattering and planar laser induced fluorescence. In the numerical part, the Rayleigh signal was generated in the simulation by using the actual species mass fractions and temperature. The analysis was first done in laminar flame and then subsequently the Rayleigh signal was incorporated in the flamelet/ progress variable (FPV) approach in a turbulent flame.

Burner and flame

Burner Design

The burner consists of two co-flows, the inner is for the oxidiser with a diameter of 95.5mm which surrounds a jet nozzle and the outer co-flow with diameter of 211.56mm is used to generate a shielding flow of air to avoid any entrainment from the surroundings. A 5mm inner diameter, 0.5mm wall

[*] Corresponding author: m.meor-zulkifli12@imperial.ac.uk

thickness nozzle with length of 100 diameters is used to ensure that the flow is fully developed when it reaches the nozzle tip. Glass beads were placed in between two perforated plates in both co-flows to produce a homogenised flow, subsequently straightened using a 100 mm tall aluminium honeycomb section. All gases were supplied from cylinders and controlled using mass flow controllers (Bronkhorst EL-Flow series) through an in-house made LABVIEW program.

Fuel and oxidizer selection

CO_2 is used to replace the N_2 in oxy-fuel combustion, which leads to up to four times higher heat loss [5]. To see the effect, numerical calculations were performed using CHEMKIN –PRO [10] showing a high quantity of O_2 is required (around 65% in the oxidiser stream by volume) to achieve desired flame temperature. However, this high proportion of oxygen also alleviates stability concerns, being well above the 30% oxygen level which has been shown to achieve air-like flame stability in previous studies [11, 12]. Soot formation also plays an important role in combustion by affecting the heat loss [5] and significantly altering chemical paths [6, 7, 8]. Wang et al. [4] found that the measured soot volume fraction in propane increases to a peak between 30% - 40% oxygen content in oxidiser and further increases of oxygen would promote soot oxidation which in turn decrease soot formation. The present experiment uses CO_2 in both the fuel and oxidiser streams, this would also further decrease the soot formation as studied by [13] where they suggested this is due to decreasing concentration of H radicals which are consumed in the reaction $CO_2 + H \leftrightarrow CO + OH$. CO_2 dilution at high temperature (2000K-3000K) was also agreed by [14] to lead to a significant decrease in soot formation. The other concern is of localised extinction that is likely to happen when the chemical reaction rate is slower than turbulent mixing which could lead to flame lift-off or blow off as CH_4 has relatively low chemical reaction rate. However as reported by [11], the addition of H_2 to the CH_4 in the fuel stream improves the global reaction rate. Our composition of fuel and oxidiser were carefully chosen by taking into account all the factors that might affect the flame stability and suitability of the flame to be investigated with the Rayleigh scattering and laser induced fluorescence techniques. Specifically, the goal was to minimise soot formation in a flame of temperature above 2400K. These broad objectives lead to composition for fuel (17.5% CH_4, 40% CO_2, 42.5% H_2) and oxidiser (68% O_2, 32% CO_2). The variation of the Rayleigh cross-section could be calculated from the numerical result from CHEMKIN-PRO and it gives a fluctuation of ±6% for this gas mixture in combustion process (from reactants to products). This large variation could not be avoided in high temperature oxy-fuel flame due to the production of CO and H_2O which gave a noticeable impact on the overall cross-section owing to their smaller cross-section compared to CO_2. In view of the magnitude of the remaining variation in cross-section it was decided to skip an attempt to perform the 'traditional' analysis to recover the temperature as demonstrated by [15, 16, 17] and instead investigate the experimental/numerical comparison of the Rayleigh signal itself.

Experimental Setup

The measurement systems used in this experiment have been described in detail in [15, 16, 17] for Rayleigh scattering and [18, 19, 20] for the OH-PLIF. As such only a brief description is provided here.

Rayleigh scattering

The Rayleigh scattering measurements were performed using the outputs of four frequency-doubled Nd:YAG laser heads (THALES Multi-channel system) at 532 nm where they were spatially overlapped, producing a combined energy of around 1.8 J/shot. The laser system was operated in burst mode, producing a batch of four sequential 10 ns duration pulses every 100 ms, and thereby limiting the peak intensity through the harmonic crystals. The polarisation of the laser output was rotated to vertical and shaped using lenses into a laser sheet with a thickness of approximately 120 µm at the centre of the imaged region and a height of 30 mm. An iris was positioned in the beam path near to the burner to block any stray light above and below the main laser sheet. The Rayleigh scattered light from the measurement volume was imaged onto an unintensified interline-transfer CCD camera (LaVision Imager Intense, set to 1µs exposure duration) using a camera lens (f/1.2, f=50 mm) and isolated with an interference filter (λ_c = 532 nm, $\Delta\lambda_{FWHM}$=3 nm). After 2 x 2 binning this yielded an imaging region of 33 mm x 25 mm with an object resolution of 50µm/pixel.

Care was taken to ensure that the measurement was not affected by stray light from the surroundings. Helium gas was flowed and imaged so that the contribution of the residual can be further removed by comparing the theoretical signal ratio of helium to oxidizer (0.00978 if no stray light present) and the one from the measurement.

The signal-to-noise ratio, SNR, was also quantified in the cold and hot regions. The cold region was taken to be the co-flow region of a turbulent flame image and SNR calculated from the ratio of the mean to the standard deviation over a 500 x 100 pixel window, while for the hot region the data was taken from pixel column 244 in a laminar flame image, corresponding to a region which gives a nearly uniform and maximal Rayleigh ratio [21]. It was found that the SNR for the cold and hot regions was approximately 36 and 13, respectively. The linearity of the camera was also verified by following the procedure described in [22] and the laser fluctuation determined from 500 oxidiser images shows a variation of only ±3%.

Planar laser-induced fluorescence

The system consisted of a dye laser (Sirah PrecisionScan) pumped by a frequency-doubled Nd:YAG laser (THALES Multi-channel system) where the pump laser was operated at 10Hz producing 532nm pulse energy of approximately 200mJ/pulse and a 10ns pulse duration. The dye laser used a Rhodamine 6G solution in ethanol. The dye beam was internally frequency doubled, producing around 5mJ/pulse in the UV. The beam was then formed into a light sheet by using a combination of a cylindrical concave and spherical convex lenses.

Different excitation and detection approaches for OH LIF imaging have been discussed in [23, 24]. In this work the $Q_1(7)$ line of the $A^2\Sigma^+$-$X^2\Pi$ (1,0) transition at around 283.2nm was excited. The fluorescence signal from the $A^2\Sigma^+$-$X^2\Pi$ (1,1) and (0,0) transitions at around 308 nm was acquired with an ICCD camera (LaVision imager intense plus IRO) with a 100 mm Halle AR-coated UV lens (f/2.0) imaging an area of 30mm x 30mm. The intensifier was gated at 200 ns to reduce background luminosity and color glass filters (1 mm thick Schott UG5 and WG305) were used to block elastic scattering at around 283nm. A mean image of laser-induced fluorescence of acetone in a quartz-cell was acquired near the jet exit, so a correction for spatial variation of the laser sheet-intensity and ICCD camera sensitivity could be performed. Background and camera noise were also corrected by subtraction of a 1000 frame ensemble average taken without laser light.

Experiment conditions

As described earlier, measurements of two different cases (laminar and turbulent) were performed in the Rayleigh experiment at two downstream regions for laminar and three for turbulent flames. For the OH-PLIF, only measurement in turbulent case was recorded. The details of the flow conditions are given in Table 1. The effect of Joule-Thompson cooling was apparent as the gas mixture in the oxidiser contains CO_2, and a large flow rate was required in the co-flow leading to a temperature drop as the flow was forced through the valves from the gas cylinder to the burner. The temperature was measured using a thermocouple both before and after each data run, so that it could be used as an input for the numerical analysis.

Table 1: Experimental Conditions

Flow Conditions	Turbulent	Laminar
Jet (kg/s)	$1.0264.10^{-4}$ (Re=18000)	$4.843{\cdot}10^{-5}$ (Re=850)
Co-flow (kg/s)	$1.052{\cdot}10^{-2}$ (U=1 m/s)	$3.157{\cdot}10^{-3}$ (U=0.3 m/s)
Ambient Temp / K	293	293
Fuel Temp / K	292	292
Oxidiser Temp / K	285	285

Numerical Approach

Laminar flame

The laminar simulation is performed as a detailed calculation evaluating the species source terms, diffusion and radiation terms directly. The governing transport equations for the density ρ, the velocity u, the total enthalpy h and the species mass fractions Y_i are

$$\frac{\partial \rho}{\partial t} + \nabla.(\rho u) = 0,$$

$$\frac{\partial}{\partial t}(\rho u) + \nabla.(\rho u u) = -\nabla p + \nabla.\tau + \rho g,$$

$$\frac{\partial}{\partial t}(\rho h) + \nabla.(\rho u h) = -\nabla + \sum_{i=1}^{I} h_i j_i + \nabla.(\lambda \nabla T) - \nabla.q_R,$$

$$\frac{\partial}{\partial t}(\rho Y_i) + \nabla.(\rho u Y_i) = -\nabla.\mathrm{j}_i + R_i,$$

where p is the pressure, τ is the laminar momentum flux, g is gravity, R_i is the chemical source term, $-\nabla \cdot q_R$ is the radiative source term and j_i is the laminar diffusive mass flux, respectively. The diffusive flux is modeled using mixture-averaged diffusion coefficients [25] with a correction velocity to ensure mass conservation. Transport contributions due to the Soret effect are included using a standard formulation, see e.g. Kee et al. [26] and are discussed in the results section below. Different radiation modeling approaches are investigated. The most simple and widely employed optically thin model with a gray absorption coefficient fit based on RADCAL simulations [27] is used here. This approach usually yields satisfactory results in standard air-combustion [28] and is thus also suggested by the TNF [29]. As a second model, the P1 approximation [30] combined with the weighted sum of gray gases (WSGG) [31] the weights from [32] is used. The latter was successfully applied in oxy-fuel combustion [33]. The laminar flame is simulated with an in-house solver based on OpenFOAM®2.1 [33, 34, 35]. The inner jet is assumed to have a Hagen-Poiseuille velocity profile and the coflow velocity is set to a block profile. The computational domain includes 1 mm of the inlet tubes and extends to a height of 150 mm with a radius of 55 mm. A 2D axisymmetric mesh with 50,000 hexahedral cells is used after grid-independence was ensured.

Turbulent flame

The turbulent simulations use the flamelet progress variable approach (FPV) [36] within the large eddy simulation framework. Transport of mass and momentum is performed by solving the Favre-filtered governing equations for the momentum $\bar{\rho}\tilde{u}$ and the governing equation for the density $\bar{\rho}$. The sub-grid scale turbulence is evaluated with the sigma model [37] applying a constant modeling constant of 1.3. For the flamelet coupling, the filtered mixture fraction $\tilde{Z}$ and its variance $\widetilde{Z''^2}$ as well as the non-normalized progress variable $\tilde{Y}_c$ are required. Transport equations for $\tilde{Z}$ and

$\tilde{Y}_c$ are solved. In contrast, based on the assumption that the sub-grid scales are locally homogeneous and in equilibrium, an algebraic equation for $\widetilde{Z''^2}$ is solved [36]

$$\frac{\partial \bar{\rho}\tilde{Z}}{\partial t} + \nabla.\left(\bar{\rho}u\tilde{Z}\right) = \nabla.\left(\bar{\rho}(D + D_t)\nabla\tilde{Z}\right)$$

$$\widetilde{Z''^2} = C_{\widetilde{Z''^2}}\Delta^2(\nabla\tilde{Z})^2$$

$$\frac{\partial \bar{\rho}\tilde{Y}_c}{\partial t} + \nabla.\left(\bar{\rho}u\tilde{Y}_c\right) = \nabla.\left(\bar{\rho}(D + D_t)\nabla\tilde{Y}_c\right) + \dot{\tilde{\omega}}_{Y_c}$$

where D_t is the turbulent diffusivity calculated with a turbulent Schmidt number of 0.4 [38, 39], D is the molecular diffusivity, Δ the filter width calculated from the cube root of the cell volume and the modeling coefficient, $C_{\widetilde{Z''^2}}$ is assumed to be 0.13 [40]. Species and temperature as well as the species properties are calculated based on the laminar flamelet concept [41] applying laminar diffusion flamelets with a discretization of 103 in the normalized progress variable, 201 in mixture fraction and 81 in the variance of the mixture fraction. The filtered density function (FDF) -integration is performed by applying a β-FDF for the mixture fraction and a δ-FDF for the normalized progress variable, assuming statistical independence [36]. For the FPV model, the choice of the progress variable is crucial [42]. In this particular flame, the single species of H2O was found to obtain a good mapping of the scalar dissipation rate to the normalized progress variable and thus $\tilde{Y}_c = \tilde{Y}_{cH2O}$.

The turbulent flame is simulated with an in-house solver based on the OpenFOAM®2.1 framework. The jet velocity inflow boundary is based on a simulation of the pipe flow in order to generate turbulent time-dependent 15 inflow profiles. These profiles are transported into the computational domain of the actual jet from the jet boundary. The coflow velocity is set to a block profile. The computational domain is a Cartesian grid of the size 30 x 30 x 150 mm at the jet inlet and enlarges to 60 x 60 x 150 mm at the outlet with a grid resolution of 64 x 64 x 300 cells, globally refined towards the nozzle. The reported statistics are collected after running the simulation for 3 flow through times (FTT) and for a period of 12 FTT.

Results and discussion

This section discusses in detail the results, both from experiment and numerical calculation. As explained in the previous section, the laminar flame calculation was studied in detail so that the influence or effect of different modelling approaches can be analyzed, while the turbulent flame result will be statistically compared.

Figure 1 shows the laminar flame Rayleigh signal from the experiment, the simulation with the P1 approach for thermal radiation, the simulation with OTM approach for thermal radiation and an adiabatic simulation. The difference is not apparent for the measurement near the burner but becomes evident further downstream. Figure 2 shows a 1D radial slice which is taken 35 mm and 75 mm from the nozzle tip to quantify the difference between these modelling approaches. The P1 approach agreed well with the experiment in terms of two-dimensional structure and absolute values due to the oxy-fuel conditions and therewith optically denser regime as discussed in [33]. On the other hand, the OTM approach seems to underestimate the Rayleigh signal but is still within the experimental uncertainty at a height of 35 mm. (The uncertainty is calculated from the standard deviation of 1000 single shots at every pixel.) Finally, the adiabatic approach overestimates the signal. The other observation that can be made from Figure 2 is that the difference in Rayleigh signal is dominated by the temperature rather than changes of species profile as there is only a minor difference especially in the lower regime, even though the difference of CO_2 is more pronounced downstream. The influence of the Soret effect was also compared to the experimental Rayleigh

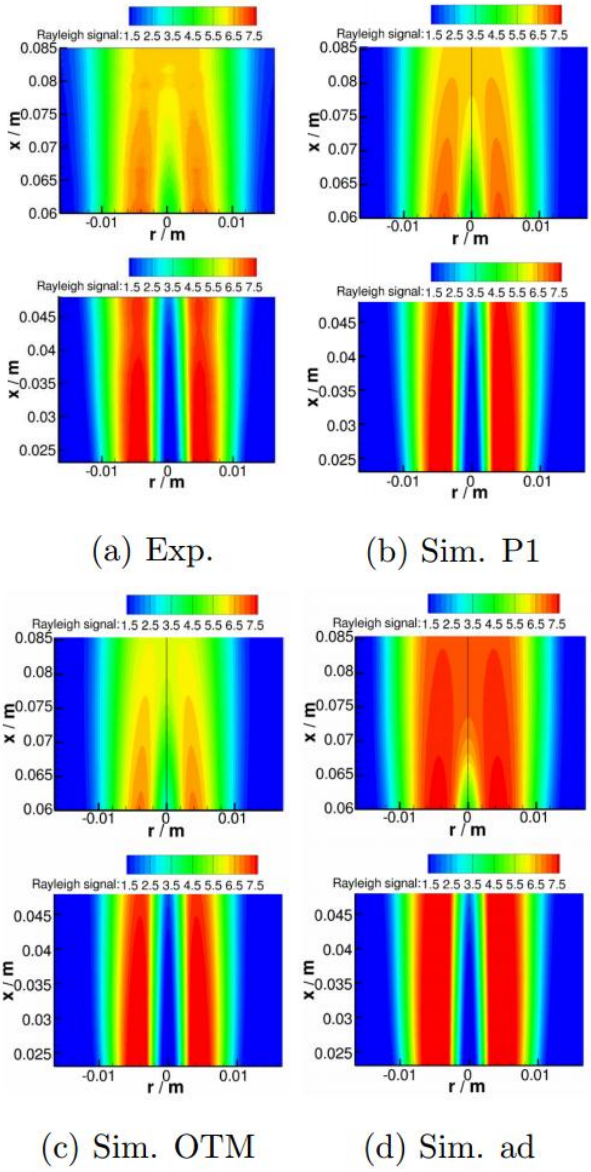

Figure 1: Rayleigh signal of the experiment and the numerical signal with different radiation models

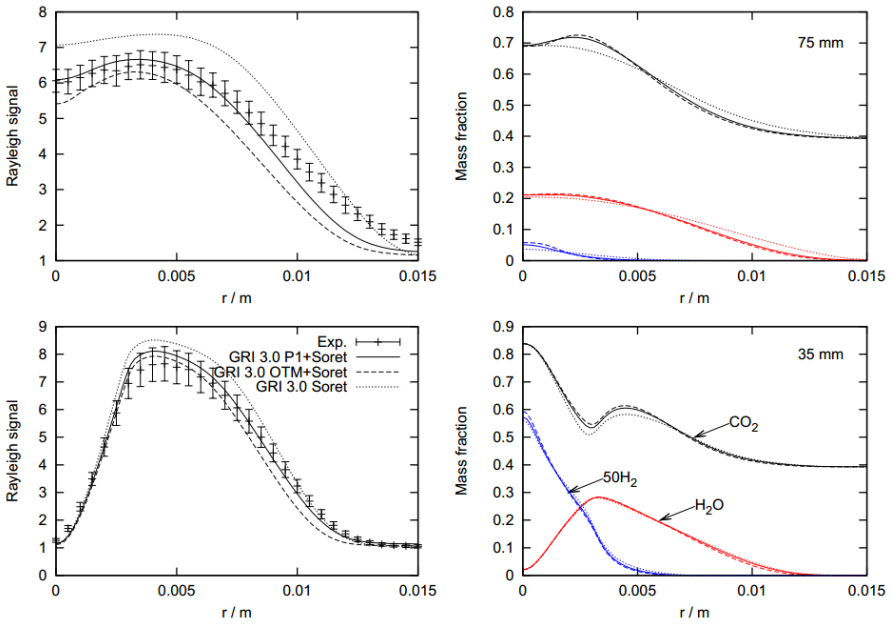

Figure 2: Comparison of the Rayleigh signal and the numerical simulation with different radiation models along a radial slice

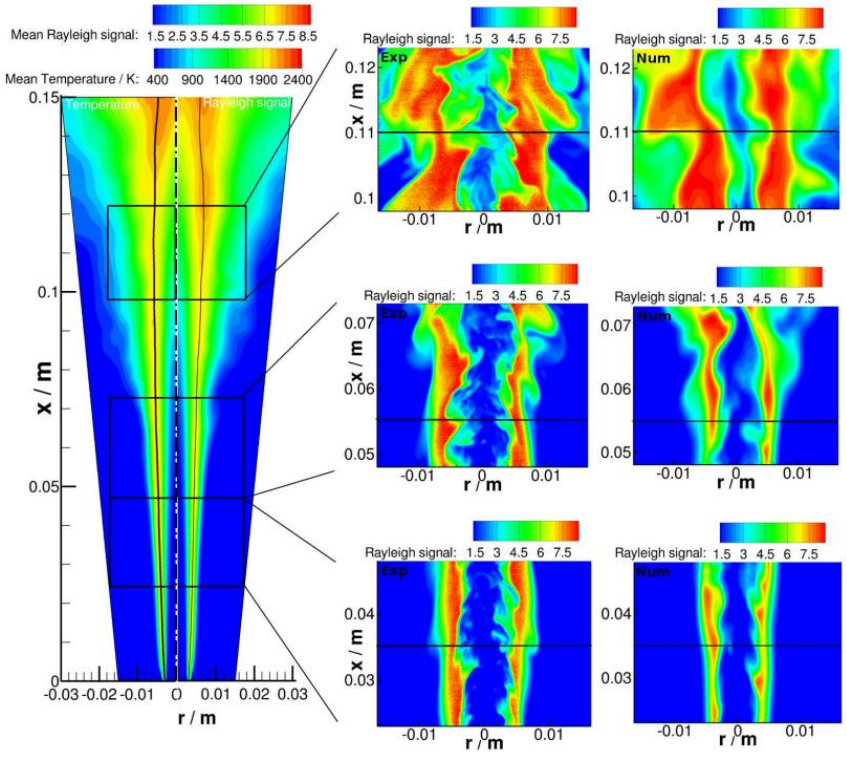

Figure 3: Contour plot of averaged temperature and Rayleigh signal, and single shot from experiment and numerical simulation

signal (not shown here). It was found out that the Soret effect has a minor influence to the experimental signal compared to the affect produced by the radiation model, as the Soret effect only shifts the species and temperature profile but not the temperature level. This effect becomes apparent in the central jet as a high H_2 concentration is used in the fuel stream and this has higher diffusivity compared to other molecules.

For the turbulent flame, a direct side-by-side comparison is impossible and so a statistical analysis is used to compare the Rayleigh signal from experiment to the numerical in terms of averaged signal, RMS and probability density function (PDF). Figure 3 shows the averaged Rayleigh signal from the simulation and a single shot comparison between the simulation and experiment. Structure-wise, the flames agreed well to each other. Further analysis could be seen in Figure 4 which compares the average, RMS and PDF of the Rayleigh signals at 35 mm, 55 mm and 110mm from the nozzle tip. The average signal in the turbulent flame shows a better agreement compared to the one in the laminar flame. At 35mm, the simulation underestimates

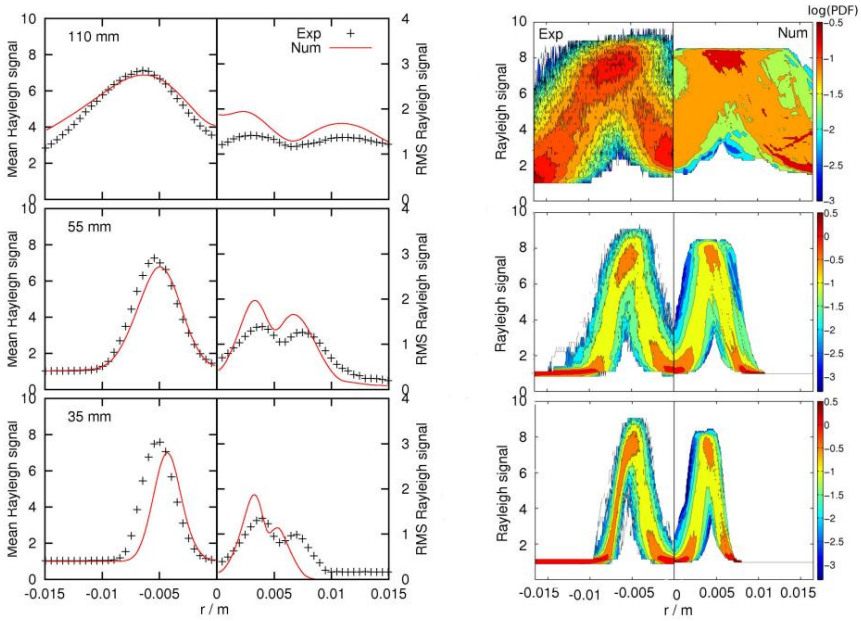

Figure 4: Comparison of mean, RMS and PDF of the Rayleigh signal from experiment and numerical simulation

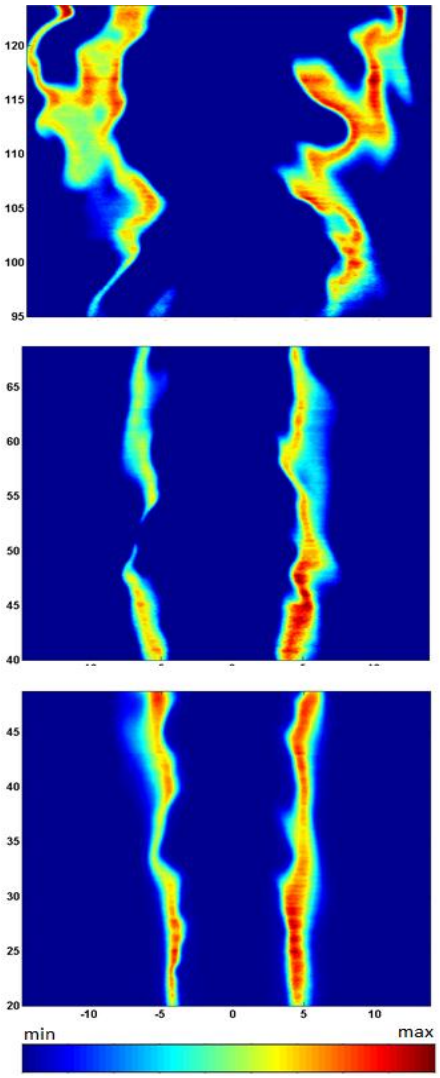

Figure 5: Single shot OH-PLIF images from the experiment

the width of the signal but improves downstream and the absolute values agree well with each other. However, for the RMS comparison, the absolute values show some overestimation at every position. In order to further investigate the statistics of the Rayleigh signal recorded in the experiments and calculated in the FPV approach, the right hand side of Figure 4 shows the PDF of the Rayleigh signal along the same slices. This representation was previously used for Rayleigh signal analysis by McManus et al. [43]. The distribution of the Rayleigh signal is shown at each point along the radius by using colour to represent the PDF values. The PDF of the numerical simulation is calculated based on approximately 15,000 snapshots, whereas the experimental PDF uses approximately 1000 snapshots. Overall, good agreement is observed. In general, the range of fluctuations increases further downstream and thus the maximum values of the PDF decrease. Further, at the heights of 35 and 55 mm the peak values of the PDF are locally very narrow, close to the peak of averaged Rayleigh signal (Avg Ray). In contrast, at a height of 110 mm a much broader range of maximum values of the PDF is found. The maximum PDF values are found varying from Avg Ray=7 to Avg Ray=8.5, and also over a broader range of radii, from r = 5mm to r=10mm.

An instantaneous image of OH-PLIF can be seen in Figure 5. The structure of this OH image is similar to the structure of the Rayleigh signal as shown in Figure 3, as the existence of OH reflects the reaction and high temperature zone. The OH distribution is not necessarily continuous as it can be seen in the middle image where there is a discontinuity at around 10 diameters above the nozzle. Such flame extinction was also reported by [11, 18]. Also, a laminar-like OH structure can be seen in the bottom image due to the effect of decreasing the local Reynolds number resulting from a high temperature which increasing the viscosity

at the upstream region. Similar to the structure in Figure 3, the OH concentration becomes broader and thicker downstream due to mixing and turbulent re-entrainment resulting from a decrease of the differential diffusion effect downstream [44].

Conclusion

An experimental study has been performed to validate the numerical simulation result in laminar and turbulent flame by using Rayleigh and OH-PLIF signal. In the laminar flame, detailed studies were performed by comparing different modeling approaches to the experimental results and the P1 radiation model approach yields a good agreement with experimental data both in structure and absolute values. For the turbulent flame, a statistical comparison was made and the resulting comparison between numerical and experimental data shows good agreement. The overall confidence in the validation of the model is significantly improved because the "traditional" Rayleigh measurement assumptions are avoided, enabling future investigations of a broad range of oxy-fuel systems.

References

[1] Wall, T.F., Proceedings of the Combustion Institute, 31(1) (2007) 31-47.

[2] Chen, L., S.Z. Yong, and A.F. Ghoniem, Progress in Energy and Combustion Science, 38 (2)(2012)156-214.

[3] Toftegaard, M.B., et al., 36(5) (2010) 581-625.

[4] L. Wang, N. E. Endrud, S. R. Turns, M. D. D'Agostini, A. G. Slavejkov, Combustion science and technology 174 (2002) 45–72.

[5] J. M. Samaniego, T. Mantel, Combustion and flame 118 (1999) 537–556.

[6] J. Park, J. S. Park, H. P. Kim, J. S. Kim, S. C. Kim, J. G. Choi, H. C. Cho, K. W. Cho, H. S. Park, Energy Fuels 21 (2007) 121–129.

[7] S. Linow, A. Dreizler, J. Janicka, E. P. Hassel, Measurement Science and Technology 13 (2002) 1952.

[8] P. Glarborg, L. L. B. Bentzen, Energy & Fuels 22 (2007) 291–296.

[9] B. Connelly, B. Bennett, M. Smooke, M. Long, Proceedings of the Combustion Institute 32 (2009) 879 – 886.

[10] R. J. Kee, F. M. Rupley, J. A. Miller, M. E. Coltrin, J. F. Grcar, E. Meeks, H. K. Moffat, A. E. Lutz, G. Dixon-Lewis, M. D. Smooke, Chemkin-pro release 15082, 2008.

[11] A. Sevault, M. Dunn, R. S. Barlow, M. Ditaranto, Combustion and Flame (2012) 3342 – 3352.

[12] M. Ditaranto, J. Hals, Combustion and flame 146 (2006) 493–512.

[13] D. X. Du, R. L. Axelbaum, C. K. Law, Proceedings of the Combustion Institute 23 (1991) 1501–1507.

[14] A. N. Mazas, D. A. Lacoste, T. Schuller, ASME Conference Pro ceedings 2010 (2010) 411–421.

[15] V. Bergmann, W. Meier, D. Wolff, W. Stricker, Applied Physics B 66 (1998) 489–502.

[16] R. W. Dibble, R. E. Hollenbach, Proceedings of the Combustion Institute 18 (1981) 1489–1499.

[17] A. C. Eckbreth, Laser Diagnostics for Combustion Temperature and Species, volume 3, Combustion Science and Technology Book Series, 1996.

[18] V. Bergmann, W. Meier, D. Wolff, W. Stricker, Applied Physics B 66 (1998) 489–502.

[19] Kiefer, J., et al., Combustion and flame, 154 (2008) 802-818.

[20] Boxx, I., et al., Combustion and Flame, 157 (2010) 1510-1525.

[21] M. Papageorge, T. McManus, F. Fuest, J. Sutton, Applied Physics B 115 (2014) 197–213.

[22] R. Hain, C. K¨ohler, C. Tropea, Experiments in Fluids 42 (2007) 403–411.

[23] K. Kohse-Höinghaus, Prog. Energy Combust. Sci. 20 (1994) 203–279.

[24] K. Kohse-Höinghaus, J.B. Jeffries (Eds.), Applied Combustion Diagnostic Taylor & Francis, New York, 2002

[25] R. B. Bird, W. E. Stewart, E. N. Lightfoot, Transport Phenomena, Wiley, 2nd edition, 2012.

[26] R. J. Kee, M. E. Coltrin, P. Glarborg, Chemically Reacting Flow, Wiley, 2005.

[27] W. L. Grosshandler, RADCAL: A Narrow-Band Model for Radiation Calculations in a Combustion Environment, Technical Report, NIST technical note 1402, 1993.

[28] R. S. Barlow, A. N. Karpetis, J. H. Frank, J.-Y. Chen, Combustion and Flame 127 (2001) 2102–2118.

[29] International workshop on measurement and computation of turbulent flames, http://www.sandia.gov/TNF/abstract.html , 2012.

[30] M. Modest, Radiative Heat Transfer, Academic Press, 3rd edition, 2013.

[31] H. C. Hottel, A. F. Sarofim, Radiative Transfer, McGraw-Hill, New York, 1967.

[32] T. Kangwanpongpan, F. H. R. Fran¸ca, R. C. da Silva, P. S. Schneider, H. J. Krautz, International Journal of Heat and Mass Transfer 55 (2012) 7419–7433.

[33] B. Garten, F. Hunger, D. Messig, B. Stelzner, D. Trimisc, C. Hasse, International Journal of Thermal Sciences 87 (2015) 68–84.

[34] F. Hunger, B. Stelzner, D. Trimis, C. Hasse, Flow, Turbulence and Combustion 90 (2013) 833–857.

[35] D. Messig, F. Hunger, J. Keller, C. Hasse, Combustion and Flame 160 (2013) 251–264.

[36] C. Pierce, P. Moin, Journal of Fluid Mechanics 504 (2004) 73–97.

[37] F. Nicoud, H. B. Toda, O. Cabrit, S. Bose, J. Lee, Physics of Fluids 23 (2011) 085106.

[38] A. Kempf, F. Flemming, J. Janicka, Proceedings of the Combustion Institute 30 (2005) 557 – 565.

[39] H. Pitsch, H. Steiner, Physics of Fluids (1994-present) 12 (2000) 2541–2554.

[40] H. Forkel, J. Janicka, Flow, Turbulence and Combustion 65 (2000) 163–175.

[41] N. Peters, Proceedings of the Combustion Institute 21 (1986) 1231–1250.

[42] M. Ihme, L. Shunn, J. Zhang, Journal of Computational Physics 231 (2012) 7715 – 7721.

[43] T. A. McManus, M. J. Papageorge, F. Fuest, J. A. Sutton, Proceedings of the Combustion Institute 35 (2014).

[44] R.S. Barlow, G.J. Fiechtner, C.D. Carter, J.Y. Chen, Combust. Flame 120 (4) (2000) 549–569.